THE INSTITUTE FOR SYSTEMS RESEARCH

ISR TECHNICAL REPORT 2018-02

Reaction Path Analysis for Atomic Layer Deposition Systems

Raymond Adomaitis

The Institute for Systems Research

A. JAMES CLARK SCHOOL OF ENGINEERING

ISR develops, applies and teaches advanced methodologies of design and analysis to solve complex, hierarchical, heterogeneous and dynamic problems of engineering technology and systems for industry and government.

ISR is a permanent institute of the University of Maryland, within the A. James Clark School of Engineering. It is a graduated National Science Foundation Engineering Research Center.

www.isr.umd.edu

Preprint for FOCAPO/CPC 2017

REACTION PATH ANALYSIS FOR ATOMIC LAYER DEPOSITION PROCESSES

Raymond A. Adomaitis*[1]

[1]Department of Chemical & Biomolecular Engineering, Institute for Systems Research, University of Maryland, College Park, MD 20742, USA

Abstract

In this paper, we examine the mathematical structure of thin-film deposition process reaction kinetics models with the goal of determining whether a reaction network can guarantee the self-limiting and stable growth inherent in true atomic layer deposition systems. This analysis is based on identifying reaction invariants and interpreting the chemical significance of these conserved modes. A species-reaction graph approach is introduced to aid in distinguishing "proper" from problematic ALD reaction networks.

Keywords

Atomic layer deposition, reaction invariants, singularly perturbed system, species-reaction graph.

Introduction

In atomic layer deposition (ALD) processes, the growth surface is exposed to cycles of alternating gas-phase precursors to produce thin solid films with atomic-level thickness control. Because of the ability of ALD to deposit an increasingly wide range of elements and compounds over topographically varying surfaces with film morphologies ranging from amorphous to crystalline (Miikkulainen *et al.*, 2013), ALD is emerging as a critical manufacturing technology for energy storage and conversion, nanoelectronics, and biomedical applications (George, 2010).

Unlike its chemical vapor deposition (CVD) counterpart, ALD processes have no steady mode of operation, and so process optimization requires kinetics models of the deposition reaction network (RN). Significant progress has been made in modeling ALD surface process from a first-principles perspective (Elliott, 2012), but studies of complete ALD RN are rare because

1. Many ALD kinetics studies are limited to a portion of the full RN (see, e.g., Travis and Adomaitis (2013)) resulting in fragmented reaction mechanisms studies;

2. There are competing reaction paths to a product species involving widely ranging, multiple time scales (Delabie *et al.*, 2012);

3. The mechanistic origins of self-limiting and steady cyclic-growth processes remains open to debate (Puurunen, 2005).

The objective of this paper is to develop the analysis tools necessary to assess whether we have an "proper" ALD reaction network before investing in the substantial effort of determining reaction rates.

Elements of an ALD reaction process

Let us consider an archetype ALD process consisting of the following overall reaction between a metal-containing precursor ML_2 and water to produce a metal-oxide film MO and gas-phase by-product HL:

$$ML_2(g) + H_2O(g) \quad \rightarrow \quad MO(b) + 2HL(g)$$

This reaction can represent, for example, the ALD of ZnO from diethyl zinc and water precursors (Gao *et al.*, 2016). The elementary reactions and net-forward reaction rates for each of the half-reactions are given in Table 1.

The first three reactions of Table 1 correspond to the metal precursor half-reaction. This simple sequence of reactions begins with the reversible adsorption of ML_2 onto the O of a surface hydroxyl group HO with net forward rate f_0 to produce the surface adduct HML_2. Because this adsorption reaction renders the O inert to

*To whom all correspondence should be addressed *adomaiti@umd.edu*

Reaction			Net rate $s^{-1}\ m^{-2}$
$ML_2(g)+2S+HO$	$\rightleftharpoons$	$HML_2+O(b)$	f_0
HML_2	$\rightleftharpoons$	$HML_2^\ddagger$	$(1/\epsilon)g_1$
$HML_2^\ddagger$	$\rightarrow$	$HL(g)+S+ML$	f_1
$H_2O(g)+ML$	$\rightleftharpoons$	$H_2OL+M(b)$	f_2
H_2OL	$\rightleftharpoons$	$H_2OL^\ddagger$	$(1/\epsilon)g_2$
$H_2OL^\ddagger$	$\rightarrow$	$HL(g)+S+HO$	f_3

Table 1. Archetype ALD process reactions and rates.

all subsequent reactions (except, of course, the desorption of ML_2), we denote the incorporation of O into the bulk film by the production of species O(b). Additionally two surface sites S are consumed by this reaction; this fictitious species accounts for the area of reaction surface that is sterically hindered by the two metal precursor ligands L. We note that gas-phase and bulk-film species are explicitly noted as such by (g) and (b), respectively, while all others are surface species.

The adsorbed adduct HML_2 can undergo a (1-2) H-transfer reaction (Delabie *et al.*, 2012) by forming the critical complex $HML_2^\ddagger$ involving the H of the hydroxyl group onto which the precursor adsorbed. We note that while conventional transition-state theory (CTST) dictates this to be an equilibrium process (Laidler, 1987), we write the net-forward reaction rate as the finite-rate process $(1/\epsilon)g_0$ using relaxation time constant ϵ for the purpose of correctly formulating the species balances that follow. The transition state $HML_2^\ddagger$ then can eliminate by-product HL(g) and liberate an adsorption site S through finite-rate process f_1, which leaves the permanently-bonded surface species ML. For this study, we consider this reaction irreversible because of sufficient reactor exhaust rate to effectively remove all HL.

The reactions corresponding to the water exposure mirror those of the metal-precursor half-cycle: water adsorbs onto the reactive metal surface species ML to form adduct H_2OL, resulting in the incorporation of metal M(b) into the bulk film. However, because there is no change in surface ligand concentration $[L]$, there is no corresponding consumption of S. Again, the surface adduct can undergo a H-transfer reaction by first forming critical complex $H_2OL^\ddagger$ in an equilibrium reaction governed by g_1, and then can undergo an irreversible reaction ejecting another HL(g), freeing one surface site S and leaving a surface HO group by finite-rate process f_3.

Before proceeding, we note that reaction rates of Table 1 can be generated from experimental measurements or quantum chemical computations coupled to conventional transition-state theory (Laidler, 1987); the analysis that follows is entirely independent of values of reaction rates f_i and the nature of the g_i.

Atoms, species, phases, and balances

The twelve species (including surface sites S) of Table 1 can be collected into chemical species set $\mathcal{S}$:

$$\mathcal{S} = \big\{\mathrm{HML_2}, \mathrm{HML_2^\ddagger}, \mathrm{H_2OL}, \mathrm{H_2OL^\ddagger}, \mathrm{ML_2(g)}, \mathrm{S}, \mathrm{HO}, \mathrm{O(b)}, \mathrm{HL(g)}, \mathrm{ML}, \mathrm{H_2O(g)}, \mathrm{M(b)}\big\}. \quad (1)$$

Clearly, three phases exist for this reaction system: the gas, surface, and bulk film phases

$$\mathcal{P} = \{\phi_0 \text{ (gas)}, \phi_1 \text{ (growth surface)}, \phi_2 \text{ (film)}\} \quad (2)$$

where ϕ_0 corresponds to the gas volume in nm^{-3} and ϕ_1 the reaction surface area in nm^{-2}. While these quantities are necessary to define the molar species balances, we are free to choose ϕ_2 to either represent the total film volume or the film surface area - the latter case is useful when we wish to represent the number of bulk species (O and M) incorporated per unit area of the growth surface. From the reactions listed in Table 1 we also can extract a set of four "elements"

$$\mathcal{E} = \{\mathrm{M}, \mathrm{O}, \mathrm{L}, \mathrm{H}\} \quad (3)$$

where the ligand L is included in $\mathcal{E}$ because it remains untransformed by any of the proposed surface reactions. As such, we note that the notation used for the chemical species in $\mathcal{S}$ can be thought of as first step towards moving to a highly simplified form of the SMILES notation (Weininger, 1988).

The thermodynamic system we study is a differential volume of constant size ϕ_0 that is perfectly uniform in each of its phases and is closed to the environment; at this time we place no restrictions on the reaction surface other than $\phi_1 > 0$ at initial conditions $t = 0$. With the species $\mathcal{S}$ (1), phases $\mathcal{P}$ (2), and the reactions, stoichiometry, and reaction rates of Table 1 in hand, we can write the twelve species differential equation balance as

$$\frac{d\mathbf{m}}{dt} = \frac{\phi_1}{\epsilon}\mathbf{P}\begin{bmatrix} g_0 \\ g_1 \end{bmatrix} + \phi_1\mathbf{Q}\begin{bmatrix} f_0 \\ f_1 \\ f_2 \\ f_3 \end{bmatrix} \quad (4)$$

with $\mathbf{m}$ being the molar amounts (*not* concentrations) of each species in $n_s \times 1$ array arranged in the ordering of (1), subject to specified initial conditions (Remmers *et al.*, 2015):

$$\mathbf{n}(t=0) = \mathbf{n}_o^A, \qquad \mathbf{n}(t=\tau^A+\tau^{AP}) = \mathbf{n}_o^B \tag{5}$$

at the start of the ML_2 (at $t = 0$) and water doses ($t = \tau^A + \tau^{AP}$) respectively, where τ^A is the length of the ML_2 exposure and τ^{AP} the post-ML_2 purge period. The stoichiometric arrays $\mathbf{P}^{n_s \times n_g}$ and $\mathbf{Q}^{n_s \times n_f}$ are:

$$\mathbf{P} = \begin{bmatrix} -1 & 0 \\ 1 & 0 \\ 0 & -1 \\ 0 & 1 \\ 0 & 0 \\ 0 & 0 \\ 0 & 0 \\ 0 & 0 \\ 0 & 0 \\ 0 & 0 \\ 0 & 0 \\ 0 & 0 \end{bmatrix}, \quad \mathbf{Q} = \begin{bmatrix} 1 & 0 & 0 & 0 \\ 0 & -1 & 0 & 0 \\ 0 & 0 & 1 & 0 \\ 0 & 0 & 0 & -1 \\ -1 & 0 & 0 & 0 \\ -2 & 1 & 0 & 1 \\ -1 & 0 & 0 & 1 \\ 1 & 0 & 0 & 0 \\ 0 & 1 & 0 & 1 \\ 0 & 1 & -1 & 0 \\ 0 & 0 & -1 & 0 \\ 0 & 0 & 1 & 0 \end{bmatrix} \tag{6}$$

Given the underlying assumption of CTST that the reactions producing critical complexes $HML^{\ddagger}$ and $H_2OL^{\ddagger}$ are in equilibrium, the true solution to (4) is found my multiplying the differential equations through by ϵ and then taking the limit $\epsilon \to 0$. Because the first four balances have nonzero entries in $\mathbf{P}$, this operation results in the loss of two equations, making it impossible to solve (4). Despite the simplicity of our archetype ALD model, computing its solution is much more complicated than one might suspect because (4) constitutes a *singularly perturbed system (STS) in non-standard form* (Daoutidis, 2015).

A "proper" ALD RN

This mechanistically simple but mathematically nontrivial model opens the question of how one defines a "proper" ALD process model. Focusing only on the intrinsic deposition kinetics, we pose the following as a subset of questions that must be asked of an RN model structure before significant effort is expended on identifying reaction rates and before precursor and by-product gas-phase transport phenomena modeling elements are incorporated to complete the deposition system description:

1. Can the reaction process time scales be separated even at the coarsest level, e.g., between equilibrium and finite-rate processes when $\epsilon \to 0$?
2. Will the model reduction process used to analyze the RN model indicate whether it will be possible to measure each finite-rate reaction process independently, or will additional information beyond the time-rate of change of species in $\mathcal{S}$ be required to determine the reaction rate values?
3. Will the deposited film have the correct stoichiometry regardless of the reaction-rate values?
4. Is the overall RN balanced, i.e., are all elemental balances satisfied for all time including the system's original state, as well as during the transitions between precursor doses and the purge periods even in the limit of infinitely fast transitions?
5. Is the deposition surface stable, e.g., will the reaction surface area have a positive and bounded value for any number of ALD deposition cycles?
6. Are self-saturating conditions guaranteed to exist, and can the mechanism be unambiguously extracted from the RN without information regarding the reaction rates?
7. Will the modes identified as being dynamically redundant have a physical meaning in the context of ALD, and can this meaning be identified as part of the reduction process?

Invariant analysis of the archetype ALD process

Because our system is closed and a balance for every species in the ALD system is provided, we should expect (4) to contain redundant dynamic modes because elements – and potentially other reaction quantities – must be conserved. Fortunately, these modes can be identified concurrently with the transformation of (4) to a STS in standard form through a reaction factorization (diagonalization) process (Adomaitis, 2016). Defining the arrays

$$\mathbf{R} = [\mathbf{P}, \mathbf{Q}]^{n_s \times n_r}, \qquad \mathbf{h} = \begin{bmatrix} \mathbf{g} \\ \mathbf{f} \end{bmatrix}^{n_s \times 1}$$

with $n_r = n_g + n_f$, we decouple the reactions through a Gauss-Jordan elimination procedure (Adomaitis, 2016; Remmers *et al.*, 2015; Rodrigues *et al.*, 2015) to as nearly as possible produce

$$\mathbf{TR} = \begin{bmatrix} \mathbf{I}^{n_r \times n_r} \\ \mathbf{0}^{(n_s - n_r) \times n_r} \end{bmatrix} \tag{7}$$

where array $\mathbf{T}$ is the matrix equivalent of the diagonalization procedure.

The objective of "nearly as possible" actually is important from a chemical kinetics point of view: under some circumstances (such as with our archetype ALD process), it is possible to achieve the transformation (7) exactly. This indicates the independence of the reactions in this reaction network (RN). However, many RN can feature elementary reaction sequences that form competing paths to the same chemical species product - these situations constitute, of course, perfectly legitimate chemical RN, and result in the inability to satisfy (7) exactly. Under these circumstances, it is sufficient to reduce (4-6) to upper-echelon form which transforms the STS to standard form, eliminates redundant dynamic modes, but does not decouple the finite-rate reaction terms (Remmers *et al.*, 2015).

The reaction factorization procedure can be carried out to completion for the archetype ALD RN (4-6) using integer arithmetic to avoid any numerical ambiguity or loss of numerical precision resulting in a diagonalized system equivalent to (7). Application of the diagonalization procedure produces $n_g = 2$ independent algebraic relationships corresponding to the equilibrium reactions, $n_f = 4$ ordinary differential equations in time corresponding to four dynamically decoupled states x_i, $i = 0, 1, 2, 3$, and $n_c = n_s - n_r = 6$ conserved quantities w_i, $i = 0, \ldots, 5$. The transformed system is given in Table 2.

The differential-algebraic equation (DAE) system of Table 2 now is in the form that can numerically solved using standard DAE solvers (e.g., an implicit-Euler scheme works very well for this relatively low-dimensional system for reaction rates f_i that do not span a wide range of timescales) provided the initial conditions marking the onset of the metal- and water-precursor doses (5) can be projected onto $g_0 = 0$ and $g_1 = 0$ (these functions are linear for the archetype ALD process, and so satisfying this condition is trivial); details regarding these numerical issues can be found in Remmers *et al.* (2015).

Given the decoupled ALD reaction model, we return to the list of criteria posed in Section for a "proper" ALD process model to examine which questions have been resolved and which remain open:

- The reaction diagonalization (factorization) procedure unambiguously determines if the pseudo-equilibrium relationships $g_i = 0$ can be solved independently at all times during the simulation, including the initial conditions, confirming condition (1) of the list.

- The new states x_i, $i = 0, \ldots, 3$ are linear combinations of the species molar quantities; these are known as reaction variants (Asbjørnsen, 1972; Rodrigues *et al.*, 2015; Zhao *et al.*, 2016). The reaction variants determine the deposition system's minimal dynamic dimension and whether those rates can be experimentally and independently measured; for the archetype ALD process, the rates can be measured independently and so condition (2) of the list is satisfied.

- The six modes w_i, $i = 0, \ldots, 5$ are known as the reaction invariants. These represent combinations of molar species quantities that remain invariant in

$$
\begin{aligned}
g_0 &= 0 \\
g_1 &= 0
\end{aligned}
$$

$$
\begin{aligned}
\frac{d}{dt}(-ML_2) &= \frac{dx_0}{dt} = f_0 \\
\frac{d}{dt}(-HML_2 - HML_2^{\ddagger} - ML_2) &= \frac{dx_1}{dt} = f_1 \\
\frac{d}{dt}(HML_2 + HML_2^{\ddagger} + H_2OL & \\
+H_2OL^{\ddagger} - ML_2 + S) &= \frac{dx_2}{dt} = f_2 \\
\frac{d}{dt}(HML_2 + HML_2^{\ddagger} - ML_2 + S) &= \frac{dx_3}{dt} = f_3
\end{aligned}
$$

$$
\begin{aligned}
-HML_2 - HML_2^{\ddagger} - S + HO &= w_0 \\
ML_2 + O &= w_1 \\
2ML_2 - S + HL &= w_2 \\
2HML_2 + 2HML_2^{\ddagger} + H_2OL & \\
+H_2OL^{\ddagger} + S + ML &= w_3 \\
HML_2 + HML_2^{\ddagger} + H_2OL & \\
+H_2OL^{\ddagger} - ML_2 + S + H_2O &= w_4 \\
-HML_2 - HML_2^{\ddagger} - H_2OL & \\
-H_2OL^{\ddagger} + ML_2 - S + M &= w_5
\end{aligned}
$$

Table 2. The archetype ALD reaction network model transformed to a singularly perturbed system in standard form, resulting in two algebraic equations, four ordinary differential equations in time, and six conserved modes.

time. Examining the w_i defined in Table 2, however, reveals little in terms of the physical meaning of these quantities. Therefore, additional analysis is required to address issues (3-7).

Species-Reaction graphs for extracting and interpreting invariants

The Species-Reaction (SR) graph was introduced by Feinberg and coworkers (Craciun and Feinberg, 2006) to facilitate analysis of chemical reaction networks to determine the potential for multiple equilibria under isothermal conditions. An SR graph is constructed from a sequence of chemical reactions according to the following format:

1. Chemical species and reactions form the nodes of the graph; species are denoted with circular nodes, reactions with square nodes. In our work, we distinguish equilibrium from finite-rate reactions using different node colors (blue and yellow, respectively), although the distinction has no bearing on the identification and interpretation of reaction invariants.

2. Species and reactions are connected by edges defined by the stoichiometry of the reactions; as such, species can only be connected to reactions so reaction-reaction and species-species edges are not possible.

3. Reaction stoichiometric coefficients are used to label the edges. In our work, negative stoichiometric coefficient values denote reactants and positive products – the sign notation can be reversed without affecting the results of our analysis.

Translation of the archetype ALD process of Table 1 (it it important to stress that the graph corresponds to the RN prior to our factorization procedure) results in the graph shown in Fig. 1. With this graph, one can visually trace the path of reaction sequences through the RN from gas-phase precursor (e.g., ML_2), through the surface reactions, to the ultimate destination of the metal atom M in the bulk film. Likewise, it also is possible to trace the multiple reaction paths that lead to the gas-phase by-product HL.

Terminal to terminal species, linear graph

Given the complexity of the archetype ALD process SR graph (Fig. 1), we now turn to examining its distinct

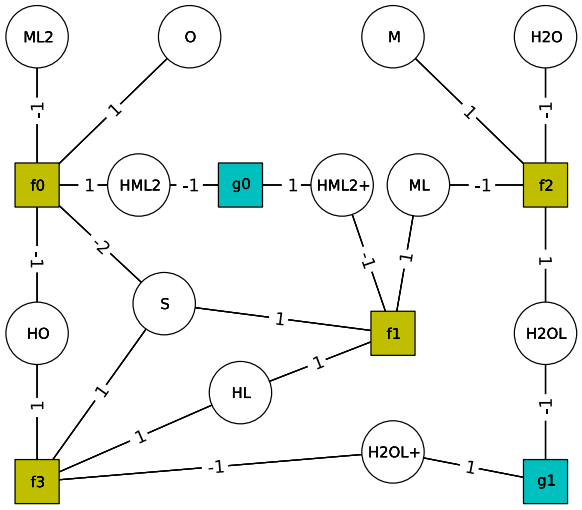

Figure 1. ALD archetype system SR graph. ML2 and H2O represent the gas-phase precursors, HL the gas-phase by-product, O and M are the bulk film components, and all other components constitute surface species. Critical complexes are denoted by a "+" suffix. Equilibrium reactions are shaded blue, while finite-rate precesses are shown in yellow.

subgraphs to determine their connections to the reaction invariants of the complete RN. To start, consider a simple dissociative adsorption process where gas-phase dimer species D(g) adsorbs dissociatively and reversibly onto a reaction surface; the physisorbed adatoms A then can undergo an irreversible incorporation into the film consisting of species B(b). The two reactions and three species are written as:

$$|\nu_{R0}|\mathrm{D(g)} \rightleftharpoons \nu_{P0}\mathrm{A} \quad \text{with net forward rate } f_0 \tag{8}$$

$$|\nu_{R1}|\mathrm{A} \rightarrow \nu_{P1}\mathrm{B} \quad \text{with rate } f_1 \tag{9}$$

with $\nu_{R0} = \nu_{R1} = -1$, $\nu_{P1} = 1$, and $\nu_{P0} = 2$. These species, reactions, and stoichiometric coefficients are shown as an SR graph in Fig. 2. Because all of the terminal nodes of this SR graph are chemical species and none is a rate process, the system is closed and so we expect at least one invariant quantity; this is easily verified by writing the three differential equation balances for species D(g), A, and B(b) and then performing the reaction diagonalization procedure. Alternatively, we can trace a path through the SR graph from the D to B nodes with molar quantities of D, A, and B to find

$$D + \frac{|\nu_{R0}|}{|\nu_{P0}|}\left[A + \frac{|\nu_{R1}|}{|\nu_{P1}|}B\right] = constant$$

$$\text{or} \quad 2D + A + B = w_0 \tag{10}$$

Physically, we interpret (10) as being equivalent to the conservation of the element deposited in the film by species B(b), where w_0 corresponds to the sum of the moles of the element in each of the species, starting from the precursor D(g) and ending with B(b).

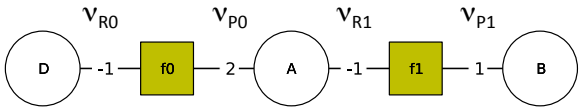

Figure 2. Linear species-reaction graph corresponding to the dissociative adsorption reactions (8-9).

Reaction branches

Now consider the SR graph of the single reaction

$$H_2 + AB \rightarrow AH + BH \tag{11}$$

shown in Fig. 3. As with the previous reaction system, all terminal nodes of the SR graph corresponding to (11) are species, and so Fig. 3 represents a closed system. There are a total of six paths we can take from one terminal species to another; diagonalization of the four species balances reveals three conserved modes and only one independent species balance. Four of the paths pass *through the reaction*:

$$\begin{aligned} \text{a)} \quad H_2 + AH &= constant \\ \text{b)} \quad H_2 + BH &= constant \\ \text{c)} \quad AB + AH &= constant \\ \text{d)} \quad AB + BH &= \text{(b) + (c) - (a)} \end{aligned}$$

and so the fourth path (d) is clearly seen as a linear combination of the first three. Two paths bypass the reaction and so constitute paths *through each reaction complex:*

$$\begin{aligned} H_2 \text{ - } AB &= \text{(a) - (c)} \\ BH \text{ - } AH &= \text{(b) - (a)} \end{aligned}$$

which are both linear combinations of the paths (a-d) passing through the reactions.

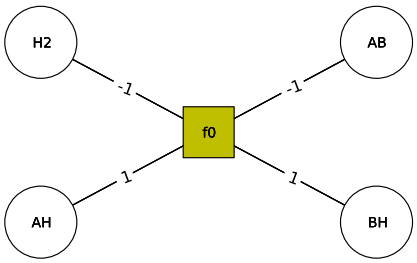

Figure 3. Reaction branch SR graph for (11).

At this point, we make one observation relevant to the interpretation of the reaction invariants of Table 2: that the negative quantities originate from reaction branches in the archetype ALD process SR graph representing paths through reaction complexes. To generate physically meaningful reaction invariants, we will only generate reaction invariants corresponding to paths passing through reactions (so the stoichiometric coefficients must change sign between the incoming and outgoing edges), and to combinations of those modes resulting from sums of invariants. For example, because (11) must produce three independent reaction invariants, we can add paths (a) and (b) and list (c) and (d) as-is to define

$$\begin{aligned} 2H_2 + AH + BH &= w_0 \\ AB + AH &= w_1 \\ AB + BH &= w_2 \end{aligned}$$

which correspond to atomistic balances of H, A, and B summing to w_0, w_1, and w_2, respectively. We observe that this path-following procedure to generate invariants in some ways can be seen as a "logical or" for the evolutionary paths of chemical species in the RN - that certain species potentially participate in one "or" more conserved relationships, and the enumeration of those paths takes place in a manner independent of other reaction paths corresponding to conserved quantities.

A final connection between well-established reaction stoichiometry relationships and reaction invariants can be observed by creating the atomic balance array A:

	H_2	AB	AH	BH	
A	0	1	1	0	(w_1)
B	0	1	0	1	(w_2)
H	2	0	1	1	(w_0)

where the nullity of A corresponds to the number of columns of A - the rank of A, which in this case has the value 1. This means the null space or kernel of A can be found as the one-dimensional vector $[-1, -1, 1, 1]^T$ which is, of course, a vector of the stoichiometric coefficients of (3).

Species branches

Next consider the RN of Fig. 4, where the primary difference relative to the previous case is that this RN branches through a species node as opposed to a reaction as in Fig. 3. As an RN, this represents the (reversible) conversion of species A to B, the latter of which can be converted to either species C or D. The selectivity to these terminal species is determined by the relative rates f_0 and f_1.

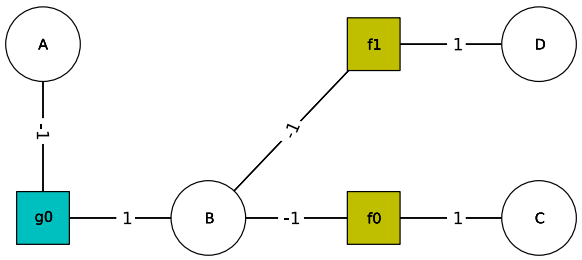

Figure 4. Species branch graph corresponding to the reaction network $A \rightleftharpoons B$, $B \to C$, $B \to D$.

Formulating the species balances and diagonalizing, we find only one reaction invariant. Conceptually, we can split the total number of A and B which ultimately are converted to C and D by defining $A = A^{(0)} + A^{(1)}$ and $B = B^{(0)} + B^{(1)}$ where superscripts (0) and (1) denote that subtotals of A and B destined to become C and D, respectively. Following each RN path from A to either C or D gives

$$A^{(0)} + B^{(0)} + C = constant \tag{12}$$

$$A^{(1)} + B^{(1)} + D = constant \tag{13}$$

$$\text{therefore} \quad A + B + C + D = w_0 \tag{14}$$

It is important to stress that because species molar amounts $A^{(0)}$, $A^{(1)}$, $B^{(0)}$ and $B^{(1)}$ are fictitious quantities, (12) and (13) are not physically realizable invariants; equation (14) is the only true reaction invariant of this RN. As such, because all paths passing through a species branch must be summed, this type of branch serves as a "logical AND" for paths through a RN.

Reaction cycles

The final RN structure we examine is the reaction cycle. Consider the sequence of reversible decomposition reactions A $\rightleftharpoons$ 2B $\rightleftharpoons$ 4C shown in Fig. 5. We close this sequence of reactions into a cycle by allowing 4C $\rightleftharpoons$ A; this is, of course, highly contrived, but that is intentional so as to make clear what role the reaction stoichiometry plays in the reaction invariant associated with this RN. We note, however, that the structure of this cyclic reaction is exactly the same as that of the isomerization reaction studied by Wei and Prater (1962).

As with the species-branching case, we split the number of one species into two artificial subtotals, such as $A = A^{(0)} + A^{(1)}$ which breaks the cycle into a terminal-to-terminal linear reaction sequence. The procedure to account for the reaction stoichiometry used in (10) then

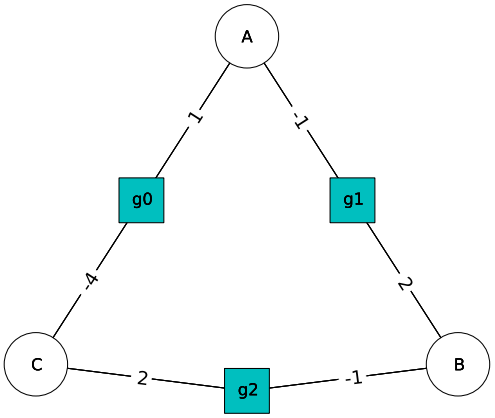

Figure 5. Reaction cycle graph for $A \rightleftharpoons 2B \rightleftharpoons 4C$.

produces the single reaction invariant

$$A^{(0)} + \frac{1}{4}\left[C + \frac{2}{1}\left[B + \frac{2}{1}A^{(1)}\right]\right] = constant$$

$$4A + 2B + C = w_0$$

Interpretation of this result makes physical sense: if species A corresponds to the element making up species B and C, w_0 represents the initial and constant number of atoms of A in the RN.

Archetype ALD process: SR graph analysis

Returning to the archetype ALD process described by the reactions of Table 1 and shown as a SR graph in Fig. 1, we now present an alternative approach to determining the six expected reaction invariants and will examine their physical meaning relative to those listed in Table 2. As seen in Fig. 6, there are two non-branching paths (shaded in blue) in this RN: one originates from the metal gas-phase precursor ML_2(g) and travels through the SR to the bulk metal M(b), while the other path originates from the O-containing precursor H_2O(g) and follows a different path to bulk film O(b). These are shown as the top two SR graphs of Fig. 6; the corresponding reaction invariants are given as w_0 and w_1 in Table 3.

Two branching paths can be seen in the lower graphs of Fig. 6. As with the M and O conservation modes, the two new paths have as one terminus either the ML_2(g) or the H_2O(g) precursor. However, each of these cases possesses a reaction branch point, where both branches lead to the HL(g) by-product (these paths are differentiated by color in Fig. 6). This ultimate confluence of reaction paths can be treated either as a species branch or as a cycle; in either case, the reaction invariant is

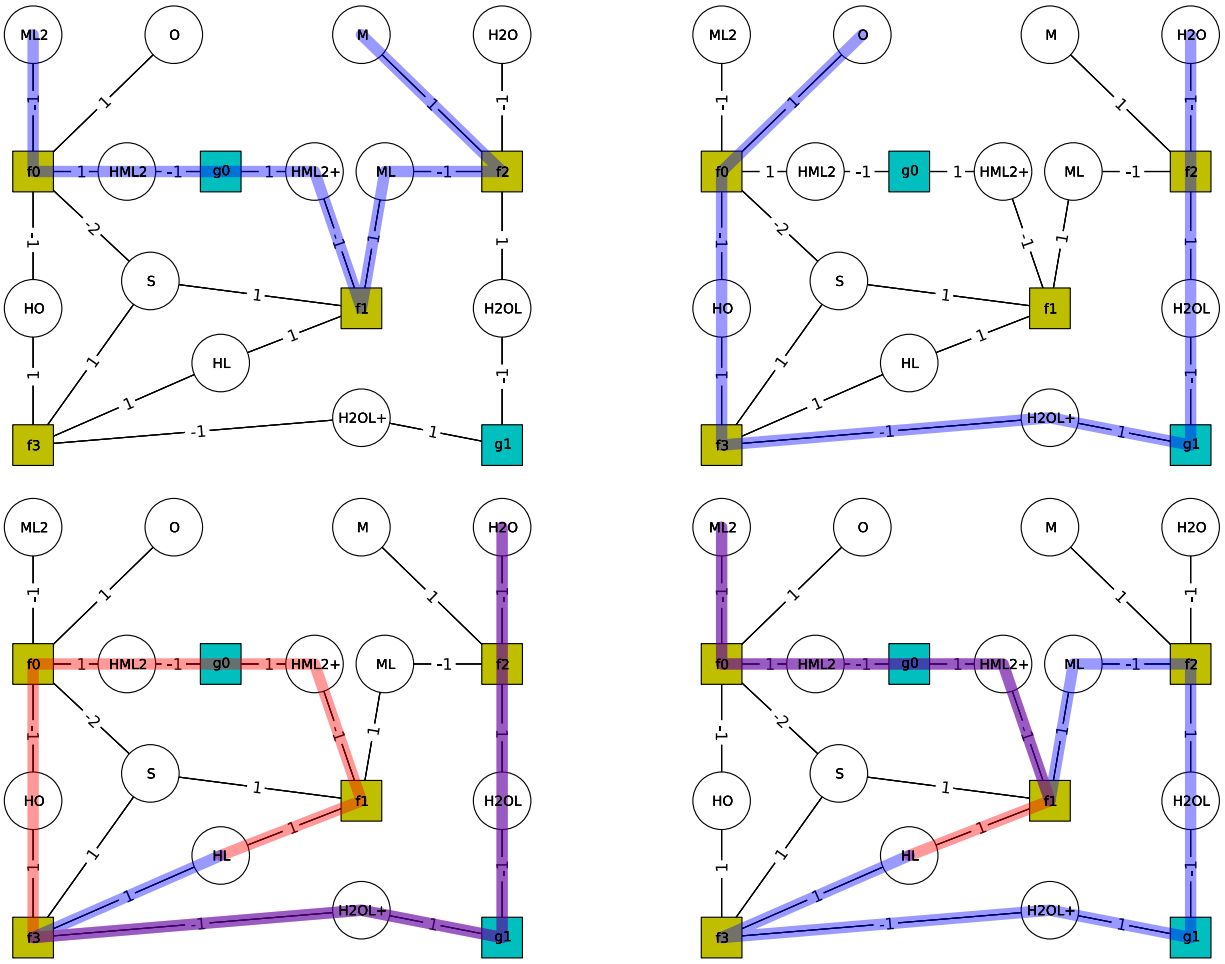

Figure 6. Archetype ALD SR graph illustrating reaction paths corresponding to M (top left), O (top right), H (bottom left), and L (bottom right) conservation.

resolved by the definition of the HL(g) molar subsets $HL = HL^{(0)} + HL^{(1)}$, allowing for the identification of two invariants for each case which are then added to eliminate the $HL^{(0)}$ and $HL^{(1)}$. This analysis results in the L and H conservation modes, defining the third and forth invariants (w_2 and w_3) of Table 3.

The surface SR subgraph

Having identified four physically meaningful and linearly independent reaction invariants, two remain to be found. To aid in this identification process and clarify the physical interpretation of these modes, we remove the gas- and bulk-phase species from the RN SR graph, leaving only the surface species and reactions. The simplified RN SR graph is shown in Figs. 7 and 8. Inspection of the SR graph limited only to surfaces processes reveals three interconnected cycles that define the two remaining reaction invariants.

Two of these cycles are shown in Fig. 7, where the overlap between the cycles consists of the S - f_0 - HML_2 - g_0 - $HML_2^{\ddagger}$ - f_1 path. Both cycles can be interpreted as closed loops of reaction processes, each consuming and then producing one unit of surface area corresponding to the size of ligand L. Thus, one cycle (depicted in red) consumes one surface site S through the formation of adsorbed HML_2 which then is transformed to critical complex $HML_2^{\ddagger}$ and then consumed to return one site S as part of this H-transfer reaction.

Likewise, the same sequence initiates the second cycle (shown in blue) corresponding to the L group not involved in the first cycle. Therefore, this cycle proceeds through the ligand-exchange path involving reactions related to the production and consumption of H_2OL, which ultimately returns the second S consumed during the ML_2(g) adsorption. As such, this overall process can be described as a species-branch process, where splitting species S to define the sum $S = S^{(0)} + S^{(1)}$ decouples the cycles and subsequently determines the reaction invari-

$$ML_2 + HML_2 + HML_2^\ddagger + ML + M = w_0 \text{ (M conservation)}$$
$$H_2O + H_2OL + H_2OL^\ddagger + HO + O = w_1 \text{ (O conservation)}$$
$$H_2O + H_2OL + H_2OL^\ddagger + HL^{(0)} +$$
$$H_2O + H_2OL + H_2OL^\ddagger + HL^{(1)} + HO + HML_2 + HML_2^\ddagger = w_2 \text{ (H conservation)}$$
$$ML_2 + HML_2 + HML_2^\ddagger + HL^{(0)} +$$
$$ML_2 + HML_2 + HML_2^\ddagger + HL^{(1)} + ML + H_2OL + H_2OL^\ddagger = w_3 \text{ (L conservation)}$$
$$HML_2 + HML_2^\ddagger + S^{(0)} +$$
$$HML_2 + HML_2^\ddagger + S^{(1)} + ML + H_2OL + H_2OL^\ddagger = w_4 \text{ (reaction area conservation)}$$
$$HML_2 + HML_2^\ddagger + ML + H_2OL + H_2OL^\ddagger + HO = w_5 \text{ (reaction site conservation)}$$

Table 3. Conserved modes for the archetype ALD reaction system. The sums $HL^{(0)} + HL^{(1)}$ and $S^{(0)} + S^{(1)}$ are replaced with HL and S, respectively, in the true invariants.

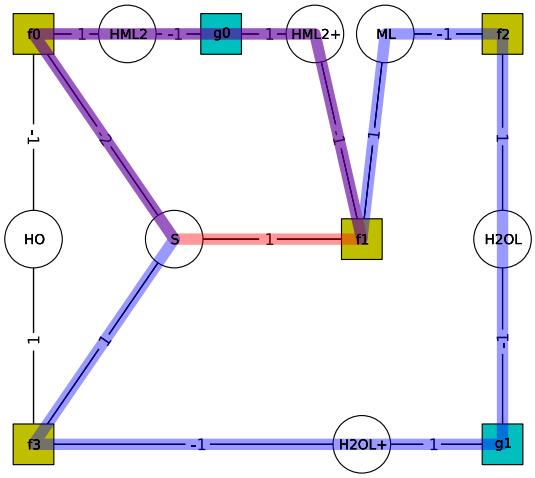

Figure 7. Surface-phase reaction surface area conservation for the archetype ALD process.

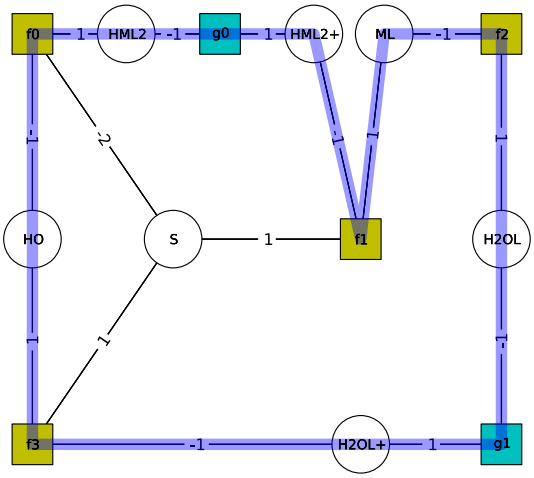

Figure 8. Surface-phase reactive site conservation for the archetype ALD process.

ant w_4 of Table 3. Defining $S = S^{(0)} + S^{(1)}$ also splits the edge between species S and reaction f_0 in the SR graph into two, each with a stoichiometric coefficient of -1.

Identification of self-limiting ALD behavior

During an exposure to the metal-containing precursor $ML_2(g)$, reaction rate $f_2 = 0$, a condition corresponding to zero H_2O adsorption rate. This effectively breaks the second cycle described above, resulting in a terminal species ML. This corresponds to the ALD growth surface for a saturating $ML_2(g)$ dose and demonstrates the self-limiting nature of a true ALD process. An alternative way of understanding this behavior is to compare it a chemical vapor deposition (CVD) reactor operating at steady state. Under this condition, one or more continuous cycles must exist containing species S to maintain open adsorption sites for the CVD precursors.

Surface site conservation

A third cycle limited to surface species and reactions can be identified that is linearly independent of the two cycles described above. As seen in Fig. 8, this clearly defined cycle does not involve S but does contain the surface hydroxyl HO. By following the reactions in this cycle, it is clear that it represents the final invariant: the conservation of reaction sites and conserved quantity w_5 of Table 3. The importance of this reaction invariant is that it guarantees the reaction surface remains bounded - that it does not growth indefinitely or vanish, halting

the reaction process. As with the the reaction invariant signaling self-limiting ALD behavior, this cycle also is broken when $f_0 = 0$ and/or $f_2 = 0$ corresponding to the individual precursor doses and purge periods.

Concluding remarks

The primary objective of this work was to define what constitutes a "proper" atomic layer deposition (ALD) reaction kinetics model through the physical interpretation of the reaction invariants. By constructing species-reaction (SR) graphs of the ALD reaction network (RN) and by developing a set of rules for extracting reaction invariants from the SR graphs, six reaction invariants were identified for our archetype ALD process. Four invariants were found to be attributed to the species elemental balances and the remaining two to reaction surface area and species conservation modes; the latter were interpreted as signals of "proper" ALD model behavior, both in terms of self-limiting ALD growth and stability of the growth surface.

This scope of this study was limited to reaction invariants; interpretation of the reaction variants in the context of the SR graphs is underway. The ALD RN models of this study correspond to closed systems and so do not account for the dynamics associated with the transport of reactants and gas-phase reaction byproducts into and from the ALD reactor vessel. While gas-phase transport will not affect the invariants associated with the surface processes, analysis of the open reaction system will be necessary to understand the complete ALD RN picture.

Acknowledgments

The author gratefully acknowledges the support of the US National Science Foundation through grants CBET1160132 and CBET1438375.

References

Adomaitis, R. A., Dynamic dimension reduction for thin-film deposition reaction network models, *Proc, IFAC DYCOPS-CAB 2016*, Trondheim, Norway 448-453 (2016).

Asbjørnsen O. A., Reaction invariants in the control of continuous chemical reactors, *Chem. Engng Sci.* **27** 709-717 (1972).

Craciun, G. and M. Feinberg, Multiple equilibria in complex chemical reaction networks: II. The species-reaction graph, *SIAM J. Appl. Math.*, **66** 1321-1338 (2006).

Daoutidis, P., DAEs in model reduction of chemical processes: An overview, *Surveys in Differential-Algebraic Equations II* A. Ilchmann and T. Reis (eds), Springer International Publishing (2015).

Delabie, A., S. Sioncke, J. Rip, S. Van Elshocht, G. Pourtois, M. Mueller, B. Beckhoff, and K. Pierloot, Reaction mechanisms for atomic layer deposition of aluminum oxide on semiconductor substrates, *J. Vac. Sci. Technol. A* **30** 01A127-1 (2012).

Elliott, S. D., Atomic-scale simulation of ALD chemistry, *Semicond. Sci. Technol.* **27** 074008 (2012).

Gao, Z., F. Wu, Y. Myung, R. Fei, R. Kanjolia, L. Yang, and P. Banerjee, Standing and sitting adlayers in atomic layer deposition of ZnO, *J. Vac. Sci. Technol. A* **34** 01A143-1–10 (2016).

George, S. M., Atomic layer deposition: An overview, *Chem. Rev.* **110** 111-131 (2010).

Laidler, K. J., *Chemical Kinetics*, Third edition Harper & Row, (1987).

Miikkulainen, V., M. Leskelä, M. Ritala and R. L. Puurunen, Crystallinity of inorganic films grown by atomic layer deposition: Overview and general trends, *J. Appl. Phys.* **113** 021301-1–101 (2013).

Puurunen, R. L., Surface chemistry of atomic layer deposition: A case study for the trimethylaluminum/water process, *Appl. Phys. Rev.* **97** 121301-52 (2005).

Remmers, E. M., C. D. Travis, and R. A. Adomaitis, Reaction factorization for the dynamic analysis of atomic layer deposition kinetics, *Chem. Engng Sci.*, **127** 374-391 (2015).

Rodrigues, D., S. Srinivasan, J. Billeter, D. Bonvin, Variant and invariant states for chemical reaction systems, *Computers and Chemical Engineering*, **73** 23-33 (2015).

Travis, C., D. and R. A. Adomaitis, Modeling alumina atomic layer deposition reaction kinetics during the trimethylaluminum exposure, *Theo. Chem. Accounts* **133** 1414-1–11 (2013).

Wei, J. and C. D. Prater, The structure and analysis of complex reaction systems, *Adv. Catalysis* **13** 203-392 (1962).

Weininger, D, SMILES, a chemical language and information system. 1. Introduction to methodology and encoding rules, *J. Chem. Inf. Comput. Sci.* **28** 31-36 (1988).

Zhao, Z., J. M. Wassick, J. Ferrio, and B. E. Ydstie, Reaction variants and invariants based observer and controller design for CSTRs, *Proc, IFAC DYCOPS-CAB 2016*, Trondheim, Norway 1091-1096 (2016).